IEEE Access
Multidisciplinary | Rapid Review | Open Access Journal

Received 8 March 2024, accepted 21 March 2024, date of publication 25 March 2024, date of current version 1 April 2024.

Digital Object Identifier 10.1109/ACCESS.2024.3381617

APPLIED RESEARCH

Comparative Evaluation of Electro-Mechanical Brake Clamping Force Estimation and Sensor Compensation Control Method for High-Speed-Train

SEUNGKOO BAEK
Department of Advanced Railroad Vehicle Division, Korea Railroad Research Institute, Uiwang-si, Gyeonggi-do 437-757, South Korea
e-mail: skbaek@krri.re.kr

This work was supported by the Research and Development Program of Korea Agency for Infrastructure Technology Advancement under Grant RS-2021-KA163309.

ABSTRACT Recently, with the emergence of electro-mechanical brake (EMB) devices, a control method for an electric motor to replace the existing pneumatic actuator has been studied. The clamping force estimation control method (ECM) from the rotor position of the motor is primarily used because sensor installation is difficult owing to the temperature increase of the friction surface of the brake disk. However, to accurately control the clamping force according to the change in the friction surface and hysteresis characteristics of the motor, it is necessary to consider the installation of a force sensor. This study deals with the installation of force sensors and the sensor compensation control method (SCCM) for the clamping force of an EMB for high-speed train applications. To evaluate the proposed method, that is, the SCCM of the EMB, static control with the wheel in the non-rotating state and dynamic control with the wheel in the rotating state were performed. In addition, static control performance evaluation was performed under the maximum clamping force reference and continuous step reference input. Comparing the two control methods, the error rate of the SCCM was improved by up to 5%. The results of evaluating the dynamic braking performance with the wheels rotating at 300 km/h showed that the SCCM had an improved deceleration pattern, and the braking speed was more than 3 s faster than that of the pneumatic braking system and ECM of the EMB.

INDEX TERMS Brake-by-wire, electro-mechanical-brake, sensor compensation control, estimation control, clamping force control, emergency brake.

I. INTRODUCTION

A railway vehicle braking system manufacturer recently introduced an EMB product with a pure electric drive system through a German railway fair, and announced that it would be applied to urban railway vehicles by the end of 2022. The EMB uses the rotational motion of the motor to move the caliper and to create a clamping force on the brake disk. Therefore, the main components of the EMB system are the brake caliper, motor, and inverter for the motor control. The EMB is being developed as an alternative to solve the complicated structure and management problems of air compressors, compressed air storage reservoirs and air piping used in the existing pneumatic brake system, aimed at the airless train of railway vehicles.

The development of initial EMB has been actively conducted in the automotive field to replace hydraulic brake [1], [2]. Automotive hydraulic brake systems have a complex hardware structure owing to oil pumps, solenoid valves, hydraulic piping, and additional braking function devices such as an anti-lock braking system (ABS) and electric parking brake (EPB), making maintenance increasingly difficult. However, the EMB system is small, has a fast braking operation speed, and can accurately control the braking

The associate editor coordinating the review of this manuscript and approving it for publication was Pinjia Zhang.

force through a cooperative function with the regenerative control system, making it suitable for future electric vehicles (EV) and hybrid electric vehicles (HEV) [3].

Owing to the development of motor and inverter manufacturing technologies, much research is being conducted to improve the performance of EMB. In particular, clamping force control and braking speed control are important factors, and research has been conducted on various control methods for motor actuators that provide faster and more accurate response than hydraulic and pneumatic braking devices.

The clamping force control of the EMB was initially studied for cascaded loops by applying position, velocity, and current controllers based on PI or PID control [4], [5], [6], [7], [8], and study results on diagnosis and tolerant control for failure that occurs when using current, speed and force sensors were presented [9], [10]. Recently, considerable research has been conducted on sensorless clamping force control owing to the difficulty in sensor installation and maintenance. A method to estimate the hysteresis characteristic curve of the clamp force from the polynomial function between the clamp force and motor position was presented [11], [12], [13], [14], [15], and a sliding mode control method to control the nonlinear characteristics of friction and deceleration performance for the entire vehicle system was also studied [16], [17], [18], [19], [20].

A model-based predictive control method applying the EMB state estimator and Kalman filter algorithm was studied for clamping force control [21], [22], [23], and clamping force control corresponding to the disturbance and nonlinear structure of the EMB was also studied [24], [25]. Observer-based techniques that estimated the clamping force based on the position and force disturbance observer for robust control [26] and data-driven method based on the motor current and voltage without speed measurement was studied [27]. In addition, the control methods using extended state observers were studied to reject disturbance such as unknown variables of EMB system [28].

These model and observer-based control methods require high-level processing hardware devices because much calculation is performed in the controller. In addition, the previously described control methods estimate the clamping force from the rotor position of the motor and were mainly applied DC motors, ball screws and gear structures with low reduction ratios, and the simulation and hardware-in-the-loop simulation (HILS) results were shown in a static state in which the braking disk does not rotate. Therefore, it is difficult to judge the validity because there are no cases of application to actual dynamic tests.

In the initial EMB development stage, it is necessary to select the capacity of the motor according to the required braking force of the train and the development of the algorithm is primarily performed in a static state. If the algorithm is validated in the static state, a dynamic braking test is conducted. A general mechanical brake is a principle in which a brake pad attached to a caliper and a disk contact each other to convert the kinetic energy of a train into thermal energy to reduce the speed of a train. Because the frictional surface of the caliper generates a high temperature of over 400°, the material hardness of the pad and disk becomes soft and wear continues to occur; thus, the clamping force is reduced compared with the reference value in the dynamic state of the wheel.

Therefore, sensorless estimation control alone has certain limitations, and feedback from a sensor that measures clamping force is required for accurate braking control. However, it is difficult to install a sensor that can withstand high temperature conditions and high pressure on the friction surface, and can easily fail even after installation.

In this study, a method for controlling the clamping force of an EMB caliper was proposed using the clamping force sensor compensation control method (SCCM) as a complement to the clamping force estimation control method (ECM). To minimize the failure of the force sensor, a sensor installation position was proposed. After the estimation control is performed using the position data of the motor rotor, and the motor position control is stabilized, the final motor position is compensated by the force sensor. It is experimentally shown that the performance is improved in terms of the error range of the clamping force in the static state test and deceleration time in the dynamic state test. This paper is organized as follows. The sensor compensated control procedure is introduced in Section II, and the performance evaluation of clamping force control in the stationary state is presented in Section III. The emergency brake test results for the dynamic state are presented in Section IV. Finally, conclusions are presented in Section V.

II. SENSOR COMPENSATED CONTROL PROCEDURE FOR EMB

In a conventional pneumatic braking systems, the pressure in a brake pipe is maintained based on a set of pneumatic reference values. If the pneumatic actuator is replaced with a motor, the motor must perform position, speed, and torque controls in the stall state. In addition, a force estimator is required to convert the position information of the motor rotor into clamping force. The PI controller was applied to the position, speed and current controllers, and the input current control reference value was calculated for efficient current control, as shown in Fig. 1.

The voltage equation of the synchronous d-q axis frame for a three-phase interior permanent magnet synchronous motor(IPMSM) is expressed as follows [29]:

$$\upsilon_{ds}^{r} = R_s i_{ds}^{r} + L_{ds}\frac{d\, i_{ds}^{r}}{dt} - \omega_r L_{qs} i_{qs}^{r} \tag{1}$$

$$\upsilon_{ds}^{r} = R_s i_{qs}^{r} + L_{qs}\frac{d\, i_{qs}^{r}}{dt} + \omega_r (L_{ds} i_{ds}^{r} + \psi_f) \tag{2}$$

where ω_r is the angular velocity, R_s is the resistance of the stator, L_{ds} and L_{qs} represent the d-q axis inductance of the stator, i_{ds}^{r} and i_{qs}^{r} are the synchronous d-q axis current of the stator, and ψ_f is the flux linkage from the permanent magnets.

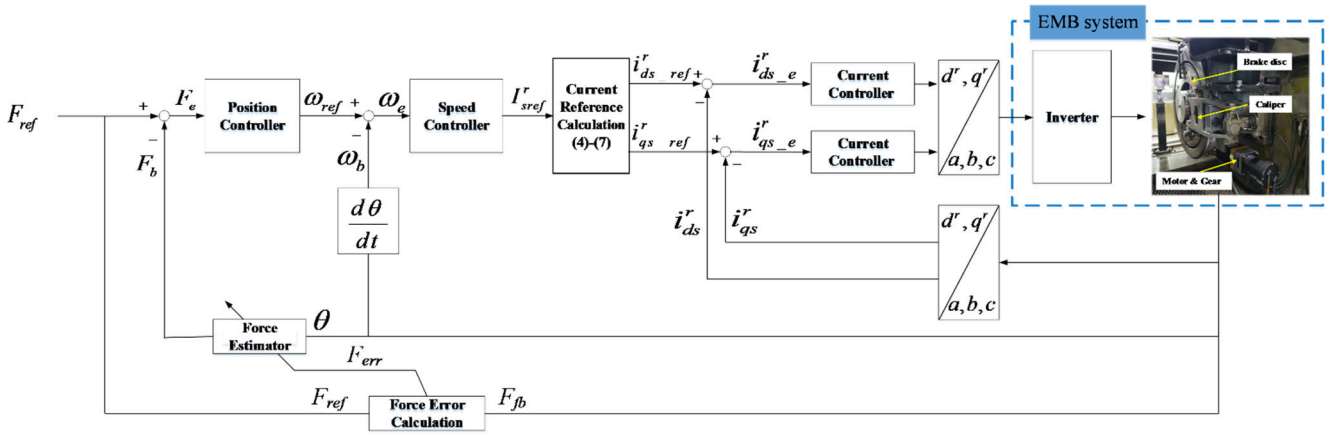

FIGURE 1. IPMSM control concept of EMB system.

From (1) and (2), the output torque of the IPMSM can be expressed as follows:

$$T_e = \frac{P}{2}\frac{3}{2}\left[\psi_f i^r_{qs} + (L_{ds} - L_{qs})\, i^r_{ds}\, i^r_{qs}\right] \tag{3}$$

where P is the number of poles

The relationship between the synchronous d-q axis frame current and angle β can be expressed as follows [30]:

$$i^r_{ds} = I_s \cos\beta\ , \quad i^r_{qs} = I_s \sin\beta \tag{4}$$

where I_s is the input current.

From (3), the output torque is expressed as I_s and β, and its derivative with respect to the β is as follows:

$$T_e = \frac{P}{2}\frac{3}{2}\left[\psi_f I_s \sin\beta + \frac{(L_{ds} - L_{qs})}{2} I_s^2 \sin 2\beta\right] \tag{5}$$

$$\frac{\partial T_e}{\partial \beta} = \frac{P}{2}\frac{3}{2}\left[\psi_f I_s \cos\beta + \frac{(L_{ds} - L_{qs})}{2} I_s^2 \cos 2\beta\right] \tag{6}$$

Because the maximum torque output occurs when (6) is zero, the value of β can be expressed as (7) [31], [32].

$$\beta = \cos^{-1}\left(\frac{-\psi_f + \sqrt{\psi_f^2 + 8(L_{ds} - L_{qs})^2 I_s^2}}{4\,(L_{ds} - L_{qs})\, I_s}\right) \tag{7}$$

Fig. 2 shows how to create a mathematical model of the force estimator applied in Fig. 1. The solid line in Fig. 2 is obtained from the test results of measuring the force according to the moving distance of the motor. A first-order model equation EST1 is applied to simplify the motor characteristic curve, as indicated by the dotted line. As a result of applying the first-order model equation, an error in the clamping force output occurrs in the mid-range between the motor characteristics and estimated model equation. However, this is not a problem because the clamping force reference value and the experimental results are within ± 5%.

When wear occurs on the brake pads, the caliper output a clamping force value that is less than the reference value when operating with the initial EST1 estimated model. In this case, the value of F_{err} increases, and if the model equation

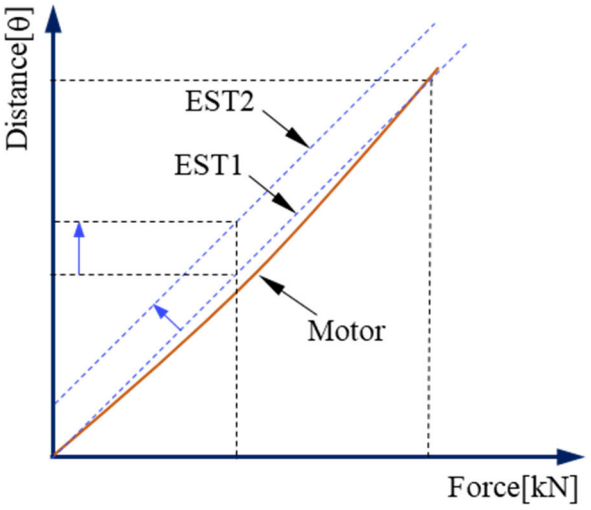

FIGURE 2. Relation between force and distance of IPMSM.

control is redefined as EST2 according to the F_{err} value, the moving distance of the IPMSM increases for the same clamping force reference input, resulting in an increase in the clamping force output value.

The error value F_{err} of the clamping force is calculated as the difference between the feedback force signal F_{fb} of the sensor measured in real time and the F_{fb} clamping force reference F_{ref}. F_{err} updates F_b which is the estimated value from the motor position θ. This control method has the advantage of improving the reliability of the EMB because it is possible to control the EMB by estimation control even if the force sensor fails.

Fig. 3 shows the structure of the EMB. The output of the motor is connected to the primary reduction gear. As the primary reduction gear rotates counterclockwise, the secondary reduction gear rotates clockwise. Because the central axis of the secondary reduction gear has a camshaft structure, the rotational motion changes to linear motion as it moves along the circumference. As lever 1 moves in the direction

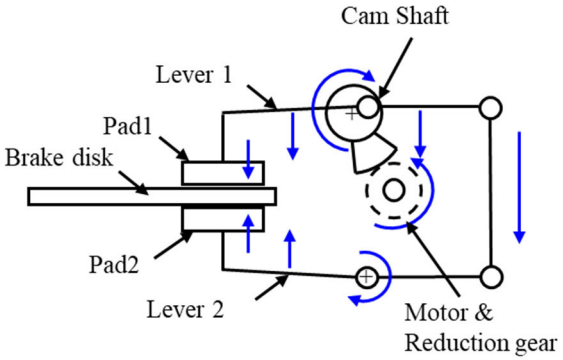

FIGURE 3. EMB structure for high-speed-train.

of the brake disk, lever 2 moves in the direction of the brake disk through mechanical coupling, creating a clamping force between the pad and disk.

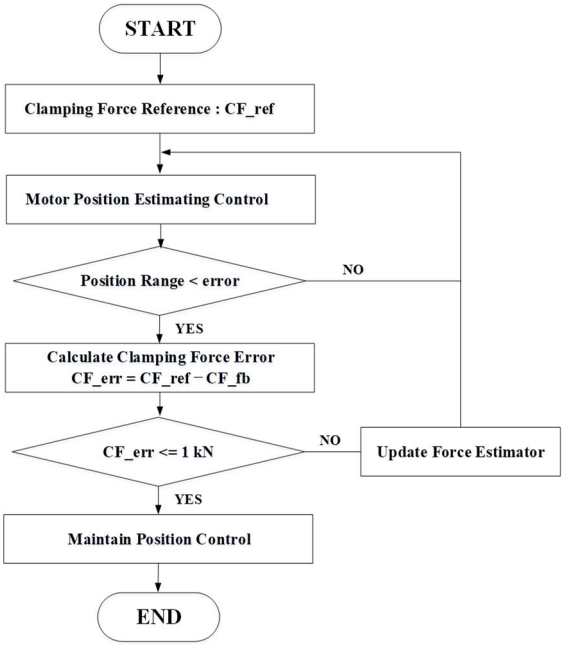

FIGURE 4. Sensor compensated control procedure for EMB clamping force.

Fig. 4 shows the SCCM procedure based on the clamping force of the ECM. When the clamping force reference is input, the EMB performs the position estimation control of the motor using the inverter, and the estimated clamping force value is within the predefined error range. At that time, the error value is calculated using the difference between the estimated force value and the measured force value; if the resulting value is less than 1 kN, the position value is maintained. If the error value exceeds 1 kN, the position control is performed again until it is less than 1 kN. When ECM and SCCM are combined, more accurate clamping force control is possible than when ECM alone is used, and reliability is improved because the braking control of the railway vehicle can be continuously maintained through estimation even in the event of sensor failure.

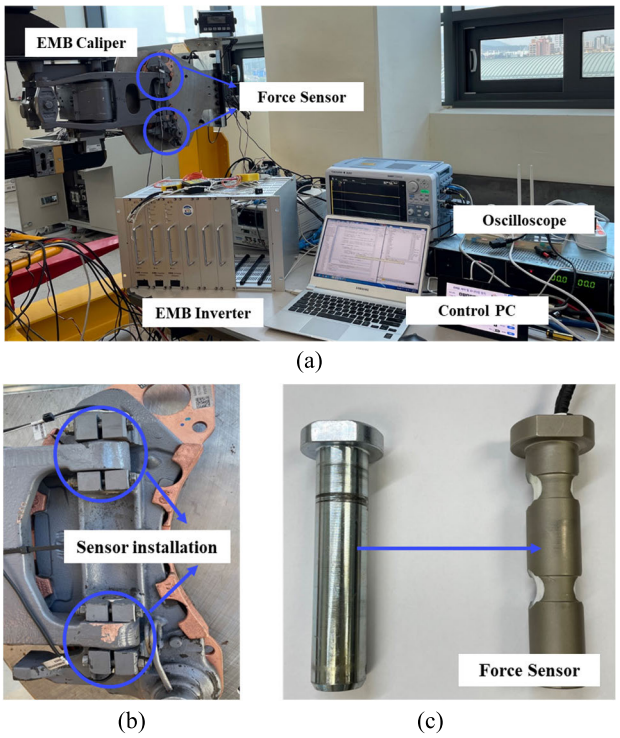

FIGURE 5. Test installation for EMB in stationary state, (a) combined test installation of EMB, (b) sensor installation position, (c) force sensor.

III. PERFORMANCE EVALUATION OF CLAMPING FORCE CONTROL IN STATIONARY STATE

Fig. 5 (a) shows the clamping force control installation of the EMB to perform a static clamping force test. A test rig sensor(loadcell) was installed inside the brake disk unit to reduce the impact of the caliper brake operation. The microprocessor control unit (MCU) for the inverter was a TMS320F28062, and the PWM switching frequency was 10 kHz. The inverter for controlling the 3-phase IPMSM uses a DC 100 V input voltage because it needs to use the battery of the train. In addition, a PC control and an oscilloscope were used to monitor the control status data and waveform.

The EMB caliper was manufactured by installing an IPMSM and reduction gear instead of a pneumatic actuator. Four sensors designed instead of bolts for measuring the clamping force were installed in the connection between the caliper arm and friction pad bracket. Fig. 5 (b) and (c) show the installation position and shape of the force sensor, respectively. A force sensor was designed to measure the force by installing a cylindrical strain gauge along the central axis of the bolt. Therefore, when the caliper arm moved inward, the force was measured based on the contact force on the disk pad. This sensor location minimizes the factors that can cause failure under high- temperature and friction conditions of the pads.

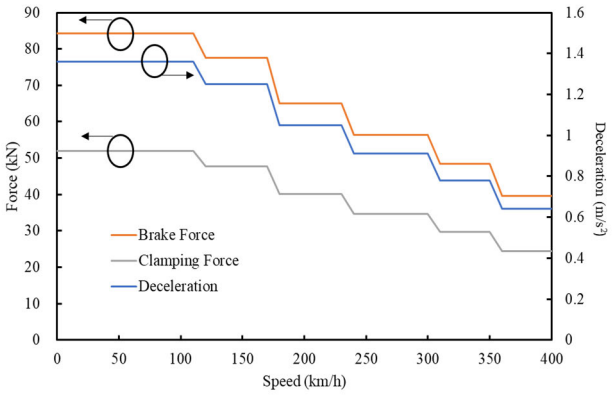

FIGURE 6. Clamping and braking force refence for HEMU-430x.

Fig. 6 shows the braking force and clamping force references according to the vehicle speed of the HEMU-430X, which was developed experimentally in Korea. As shown in Fig. 6, the braking force was determined by multiplying the weight of the train by the required deceration value. In addition, the clamping force reference of the caliper was calculated by dividing the braking force by the wheel diameter ratio and friction coefficient. The clamping force reference of the caliper started with a low clamping force input and gradually increased as the train speed decreased. This is because the high braking force at high speed causes a high temperature on the disk surface and thermal shock on the wheel, resulting in brake system failure. In addition, the braking force was determined by multiplying the weight of the train by the required deceration value.

The specifications of the IPMSM considering the braking force based on the weight of high-speed trains are listed in Table 1. The rated speed of the motor was designed to reach the maximum clamping force reference of 0.5 s. The IPMSM output is determined by the required rotational angular speed and the two-stage reduction gear ratio, as shown in Fig. 3.

TABLE 1. Motor specification.

Motor Specification	
Output power	1000 W
Rated speed	3,000 rpm
Resistance R_s	0.195 Ω
Inductance L_d	2.8×10^{-3} H
Inductance L_q	5.4×10^{-3} H
Rated current	15 A
Rated torque	3.2 Nm
Number of phase	3
Input voltage	100 V

Fig. 7 shows the static clamping force control results obtained using the ECM. The force in Fig. 7 (a) shows the measured clamping force from the sensor in the experimental installation rig in Fig. 5, where is the estimated position value corresponding to the required force reference, and the

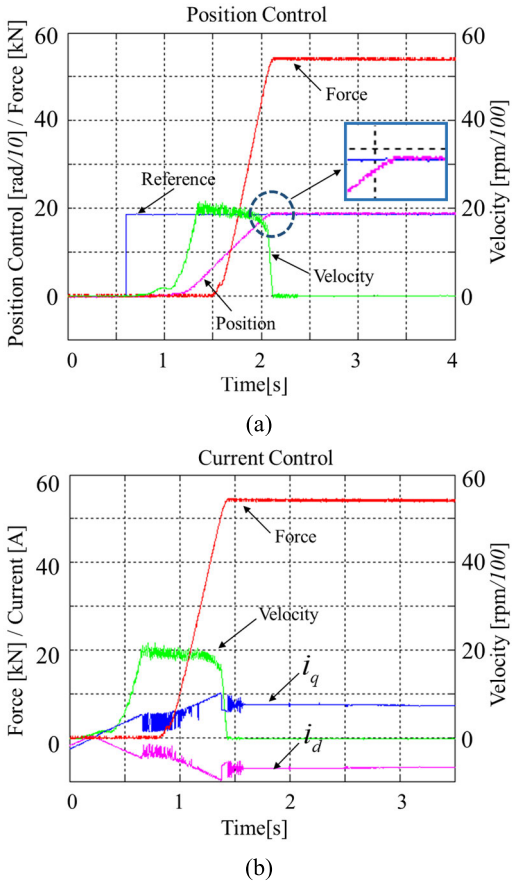

FIGURE 7. Experimental result with the static clamping force using the ECM, (a) Position control, (b) d-q axis current control.

motor starts rotating within 100 ms of the reference input. From (3), a theroretical maximum speed can be expressed as follows [30]:

$$\omega_{max} = \frac{V_{smax}}{\psi_f} \tag{8}$$

where ω_{max} is the maximum angular velocity, V_{smax} is the maximum phase voltage, and ψ_f is the flux linkage from the permanent magnets.

To reduce the overshoot of the clamping force, the maximum rotation speed of the motor was limited to 2,000 rpm, and the measured clamping force value increased slowly owing to the gap between the braking pad and the disk. When the clamping force reached the maximum value, the speed of the motor decreased to zero, and position control was performed to maintain the position. As shown in Fig. 7 (a), a maximum clamping force of 54 kN was maintained using the ECM. Fig. 7 (b) shows the d-q axis control current for the IPMSM control during the maximum clamping force. The current reference calculation in (4) was applied to improve the efficiency of the current control, as shown in Fig. 1. It was be confirmed that the motor operated as soon as the control current was input. A current of approximately 8 A for the

q-axis and approximately −7 A for the d-axis was output after the position of the motor was stabilized.

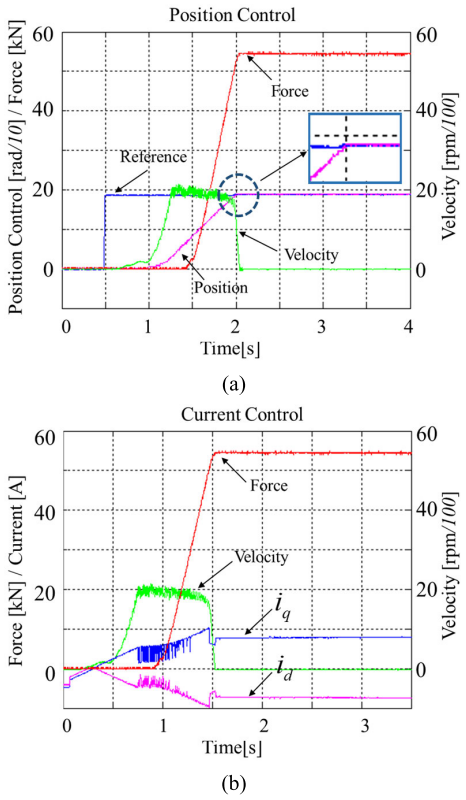

FIGURE 8. Experimental result with the static clamping force using the SCCM, (a) Position control, (b) d-q axis current control.

Fig. 8 shows the static clamping force control results obtained using the SCCM. The maximum clamping force was 54 kN, which is the same as that shown in Fig. 7 (a). The position reference in Fig. 7 (a) maintained the initial value. However, Fig. 8 (a) shows the compensated position reference obtained by slightly increasing the reference position with the sensor feedback value. The d-q axis current control in Fig. 8 (b) shows the same maximum peak current and steady-state current in the motor stall state, as shown in Fig. 7 (b).

Figure 9 shows the d-q axis output current tracking control characteristics of the current controller for the reference current calculated from (4). As shown in Fig. 1, the input reference current is determined according to the output of cascade structure of the position and speed controller. When the IPMSM reaches the maximum speed of 2,000 rpm, the reference current fluctuate to maintain the speed, and when the reference clamping force is reached, the d-q axis current follows a constant reference current to maintain the clamping force. As can be seen in the enlarged graph of the region where the reference current fluctuates in Figure 9, the d-q axis current reaches the reference current at a rapid speed within 3 ms.

As shown in previous experimental results, the output clamping force control results for the maximum reference

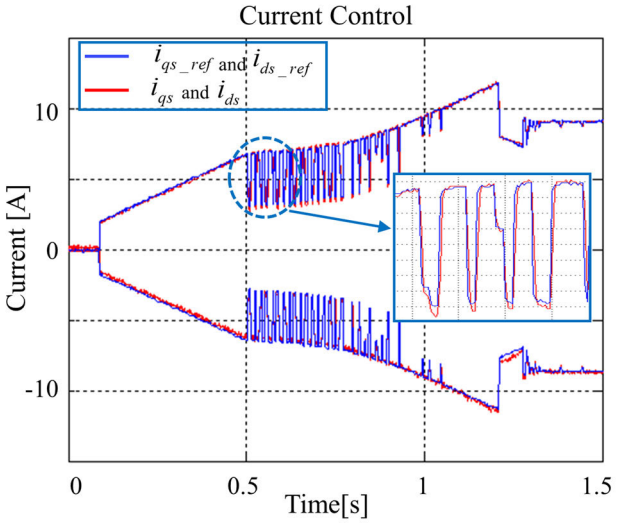

FIGURE 9. Output current characteristics tracking the d-q axis reference control current.

input force or reference input for each stage did not exhibit a significant difference in the output error values of the two control methods. However, there was a difference in the output error based on the continuous clamping force reference input at each stage.

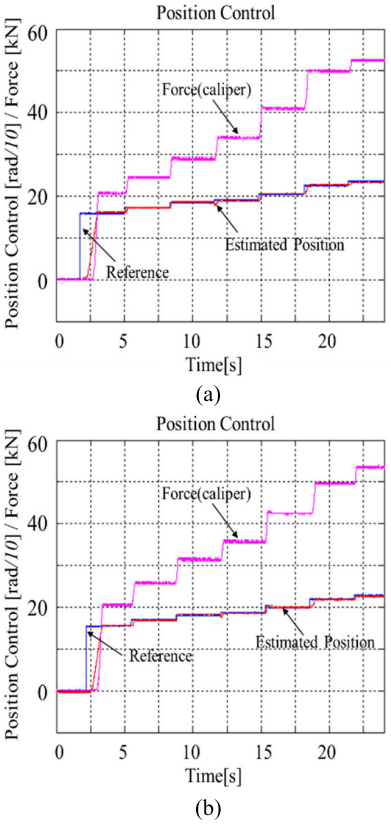

FIGURE 10. EMB ascending step position control pattern under static condition, (a) ECM, (b) SCCM.

The output of the clamping force for the continuously ascending step reference input is shown in Fig. 10. Unlike the

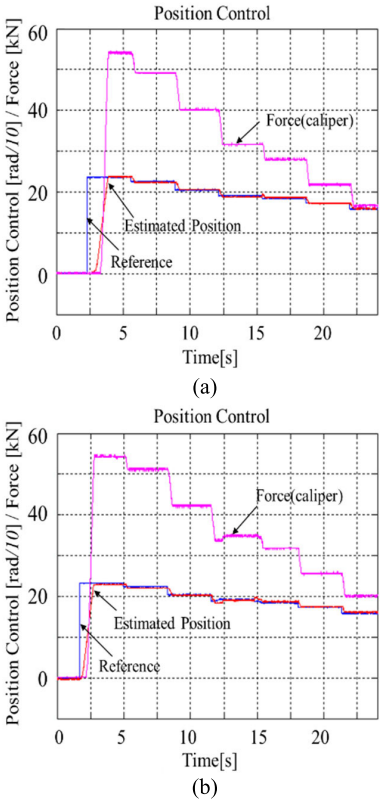

FIGURE 11. EMB descending step position control pattern under static condition, (a) ECM, (b) SCCM.

clamping force output, which increases from zero to the target clamping force in one step, this test generates the clamping force output in several steps. Fig. 10 (a) shows the results of the ECM and Fig. 10 (b) shows the results of the SCCM. As shown in Fig. 10, when the ECM is applied, the clamping force output values of steps 1-2 and steps 6-7 obtain output values that satisfy the reference values. However, the output values of clamping force steps 3 to 5 were approximately 2 kN lower than the reference value output, according to the characteristics shown in Fig. 2. In case of the SCCM in Fig. 10 (b), it can be verified that errors within ±0.5 kN are shown for all braking steps. Therefore, it can be seen that the correction of the reference value estimated through the sensor compensation is performed, and the control of the motor accurately follows the compensated reference value.

Fig. 11 shows the output of the clamping force for the continuous descending step reference input. Fig. 10 (a) shows the results of the ECM, and Fig. 10 (b) shows the results of the SCCM. In the case of the ECM, output differences continue to occur between the reference inputs and clamping forces, except for the first step 7.

This result was attributed to an error caused by the repulsive force generated in the caliper during the braking release operation of the motor. However, the SCCM receives feedback from the clamping force sensor value and readjusts the position of the motor to output each reference value of the clamping force accurately. In particular, when descending from step 5 to step 4, the error between the estimated and measured values was calculated to readjust the position of the motor, which caused an undershoot as shown in Fig. 11 (b).

Table 2 lists the results of the clamping force output values and the error between ECM and SCCM, as shown in Fig. 10. When ECM was applied, the error value of the clamping force was up to 6.5%, and the average error value of all steps was approximately 3.1%. When the SCCM proposed in this study was applied, the error value of the clamping force occurred up to 1.5%, and the average value was approximately 0.5%.

TABLE 2. Comparison of the experimental result.

Step (Reference [kN])	Test Result [kN]		Error [%]	
	Estimation control	Sensor compensated control	Estimation control	Sensor compensated control
1(20)	20.7	20.3	3.5	1.5
2(26)	24.3	26.0	6.5	0
3(31)	29.3	31.3	5.4	1.0
4(36)	34.3	36.0	4.7	0
5(42)	41.3	42.0	1.6	0
6(50)	50.0	49.7	0	0.6
7(54)	52.7	53.7	2.4	0.6

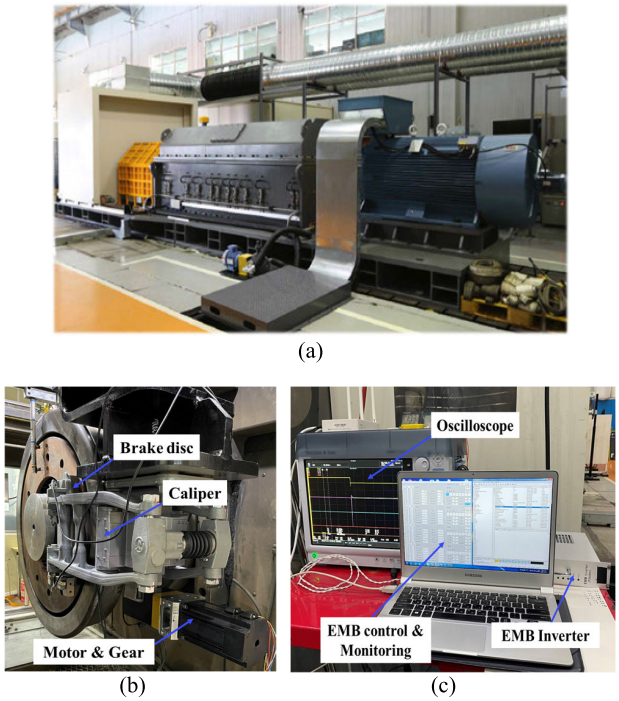

FIGURE 12. Test installation for EMB emergency brake in dynamic state test, (a) equipment for braking performance test, (b) EMB installation, (c) brake control and monitoring.

IV. PERFORMACE EVALUATION OF EMERGENCY BRAKE IN DYNAMIC STATE

Fig. 12 (a) shows the dynamo equipment for the emergency braking test, and Fig. 12 (b) and 12 (c) show the installation of the EMB performance test. A dynamic emergency

braking test of the EMB was conducted using the same testing procedure as that used for the pneumatic brake. The wheelset shown in Fig. 12 (b) was rotated at a maximum speed of 300 km/h. At that time, the clamping force of the EMB was applied as 36 kN(step 4). A clamping force of 42 kN(step 5) was applied when the wheelset speed decreased to 230 km/h and a clamping force of 50 kN(step 6) was applied when the wheelset speed decreased to 160 km/h. When the wheelset speed decreased to 110 km/h, a clamping force of 54 kN(step 7) was applied and maintained until the wheelset speed reached to 0 km/h.

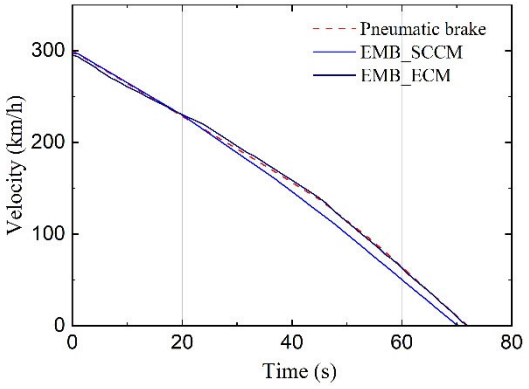

FIGURE 13. Comparison of the velocity pattern between pneumatic brake and EMB.

Fig. 13 shows a comparison of the brake performance between the pneumatic brake and EMB applied to ECM and SCCM. The pneumatic brake used was a HEMU-430X brake system.

The EMB system applying ECM showed similar results to the pneumatic brake because the two systems performed open-loop control of the clamping force value. The EMB system applying SCCM decelerated linearly at a speed of 230 km/h(step 5), and braking was completed in 69 s. However, the pneumatic brake and EMB system applying ECM were completed in 72 s. The SCCM performs the best among the three cases because the deterioration of the clapming force performance owinge to the heat on the disk surface can be controlled through sensing feedback.

Fig. 14 shows the deceleration value of each step of the SCCM, as shown in Fig. 13. As shown in the reference value for each speed range in Fig. 6, the deceleration test value satisfied the reference value in the speed range of 300 km/h to 0 km/h.

Fig. 15 shows the control waveform of the SCCM from the EMB inverter. The upper waveform is the force-sensing feedback value received from the sensor for each clamping force reference value, and the lower waveform is the speed at which the motor rotates in the forward or backward direction to control the pad position based on the clamping force feedback value. The EMB's force feedback data show a fluctuating waveform owing to the influence of noise as the vibration of the wheel rotating at high speed is transmitted to the caliper, but it follows the clamping force reference value well.

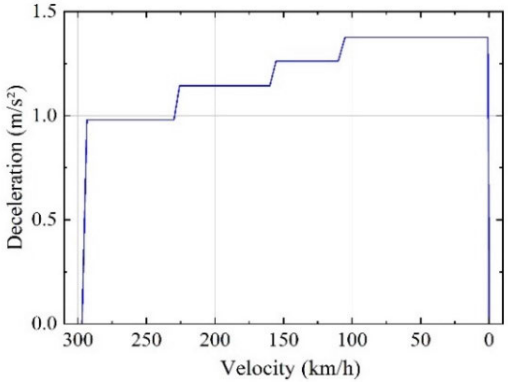

FIGURE 14. Calcuation result of EMB deceleration from velocity parttern of SCCM.

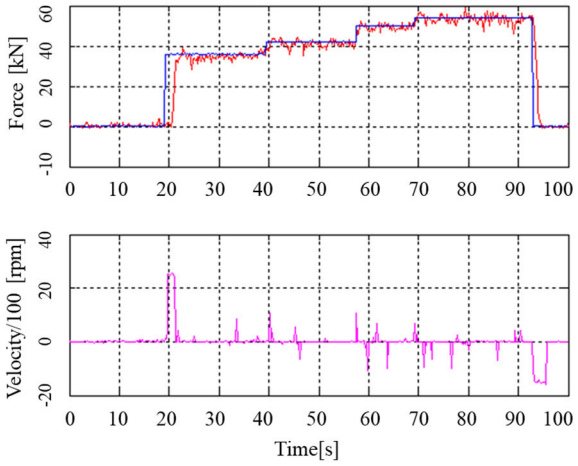

FIGURE 15. Control waveform of the SCCM from EMB inverter.

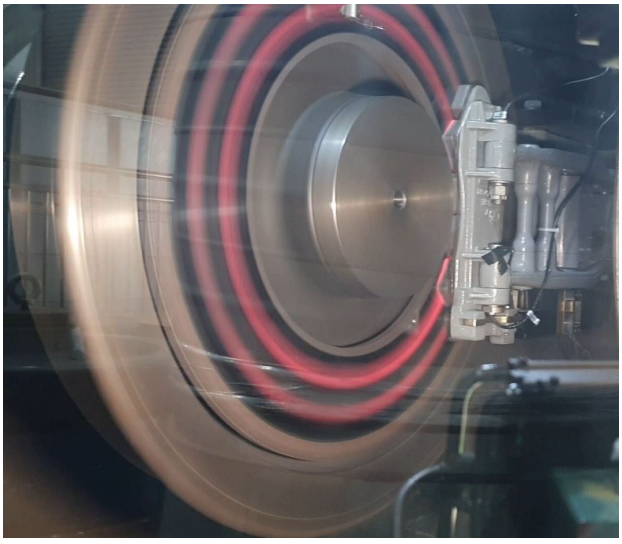

FIGURE 16. Emergency brake experiment at 300 km/h wheel velocity.

Fig. 16 shows the state in which emergency braking of the EMB is applied, while the speed of the wheelset is 300 km/h. As described in the previous section, when a clamping force

is applied by the caliper when the wheelset rotates, frictional heat is generated on the wheel disk, and a circular red band appears on the circumferential surface of the disk.

V. CONCLUSION

In this study, a force sensor installation and SCCM were used to provide a new design scheme to control the clamping force of an EMB for application to high-speed trains. The force sensor location minimizes the occurrence of failures due to environmental factors, and the control method is expected to improve the reliability of the EMB through redundancy of estimation control even in the event of a sensor failure during railway vehicle operation.

In the stationary state test, the ECM and SCCM methods yielded similar results for a one-step reference, such as the maximum reference. However, with a continuous step reference input, the clamping force error of the SCCM was improved by up to 5% compared of the ECM. In the dynamic state test, the SCCM exhibited linear deceleration characteristics for each speed range and was 3 s faster than the ECM under the same test conditions.

The main contribution is summarized in the following aspects:

- Derivation of estimation and sensor compensation control method to improve the accuracy and reliability of the EMB for high-speed train.
- Presentation of installation method considering minimization of sensor failure in high-speed, high-temperature environmental conditions.
- Derivation of procedures for combination testing in a stationary state and performance testing in a dynamic state for applying EMB to high-speed train.

When sensors are applied, frequent maintenance problems and the causes of failure increase. However, estimation control alone does not provide accurate clamping force control, and it is difficult to achieve good performance compared with existing pneumatic brake systems.

In the future, an EMB system that applies the proposed algorithm will be installed in railway vehicles and a comparative evaluation with a pneumatic braking system will be conducted.

ACKNOWLEDGMENT

The author would like to thank the Editors and the Reviewers for their contribution.

REFERENCES

[1] R. Bannatyne, "Advances and challenges in electronic braking control technology," SAE Tech. Paper 982244, 1998, doi: 10.4271/982244.
[2] M. Sundar and D. Plunkett, "Brake-by-wire, motivation and engineering—GM sequel," SAE Tech. Paper 2006-01-3194, 2006, doi: 10.4271/2006-01-3194.
[3] X. Gong, W. Ge, J. Yan, Y. Zhang, and X. Gongye, "Review on the development, control method and application prospect of brake-by-wire actuator," *Actuators*, vol. 9, no. 1, p. 15, Mar. 2020.
[4] R. Schwarz et al., "Modeling and control of an electromechanical disk brake," SAE Tech. Paper 980600, 1998, doi: 10.4271/980600.
[5] C. Line, C. Manzie, and M. C. Good, "Electromechanical brake modeling and control: From PI to MPC," *IEEE Trans. Control Syst. Technol.*, vol. 16, no. 3, pp. 446–457, May 2008, doi: 10.1109/TCST.2007.908200.
[6] C. Line, C. Manzie, and M. Good, "Control of an electromechanical brake for automotive brake-by-wire systems with an adapted motion control architecture," SAE Tech. Paper 2004-01-2050, 2004, doi: 10.4271/2004-01-2050.
[7] R. Isermann, "Electromechanical disc brake (EMB)," in *Mechatronic Systems Fundamentals*. London, U.K.: Springer-Verlag, 2003, pp. 560–568.
[8] J. K. Ahn, K. H. Jung, D. H. Kim, H. B. Jin, H. S. Kim, and S. H. Hwang, "Analysis of a regenerative braking system for hybrid electric vehicles using an electro-mechanical brake," *Int. J. Automot. Technol.*, vol. 10, no. 2, pp. 229–234, Apr. 2009.
[9] K.-J. Han, I.-J. Yang, and K.-S. Huh, "Current and force sensor fault detection algorithm for clamping force control of electro-mechanical brake," *J. Inst. Control, Robot. Syst.*, vol. 17, no. 11, pp. 1145–1153, Nov. 2011, doi: 10.5302/j.icros.2011.17.11.1145.
[10] W. Hwang and K. Huh, "Fault detection and estimation for electromechanical brake systems using parity space approach," *J. Dyn. Syst., Meas., Control*, vol. 137, no. 1, pp. 014504–014510, Jan. 2015, doi: 10.1115/1.4028184.
[11] Y. H. Ki, K. J. Lee, J. S. Cheon, and H. S. Ahn, "Design and implementation of a new clamping force estimator in electro-mechanical brake systems," *Int. J. Automot. Technol.*, vol. 14, no. 5, pp. 739–745, Oct. 2013.
[12] G. Park, S. Choi, and D. Hyun, "Clamping force estimation based on hysteresis modeling for electro-mechanical brakes," *Int. J. Automot. Technol.*, vol. 18, no. 5, pp. 883–890, Oct. 2017.
[13] Y. Li, T. Shim, D.-H. Shin, S. Lee, and S. Jin, "Effective clamping force control for electromechanical brake system," in *Proc. IEEE/ASME Int. Conf. Adv. Intell. Mechatronics (AIM)*, Boston, MA, USA, Jul. 2020, pp. 643–648.
[14] Z. Wei, J. Xu, and D. Halim, "Clamping force control of sensorless electro-mechanical brake actuator," in *Proc. IEEE Int. Conf. Mechtron. Automat. (ICMA)*, Takamatsu, Japan, 2017, pp. 764–769, doi: 10.1109/ICMA.2017.8015912.
[15] S. Saric, A. Bab-Hadiashar, and R. Hoseinnezhad, "Clamp-force estimation for a brake-by-wire system: A sensor-fusion approach," *IEEE Trans. Veh. Technol.*, vol. 57, no. 2, pp. 778–786, Mar. 2008.
[16] M. R. A. Atia, S. A. Haggag, and A. M. M. Kamal, "Enhanced electromechanical brake-by-wire system using sliding mode controller," *J. Dyn. Syst., Meas., Control*, vol. 138, no. 4, pp. 041003–041009, Feb. 2016.
[17] B. Liang, Y. Zhu, Y. Li, P. He, and W. Li, "Adaptive nonsingular fast terminal sliding mode control for braking systems with electro-mechanical actuators based on radial basis function," *Energies*, vol. 10, no. 10, p. 1637, Oct. 2017, doi: 10.3390/en10101637.
[18] W.-L. Zhu, X. Yang, F. Duan, Z. Zhu, and B.-F. Ju, "Design and adaptive terminal sliding mode control of a fast tool servo system for diamond machining of freeform surfaces," *IEEE Trans. Ind. Electron.*, vol. 66, no. 6, pp. 4912–4922, Jun. 2019, doi: 10.1109/TIE.2017.2786281.
[19] Y. Zhao, H. Lin, and B. Li, "Sliding-mode clamping force control of electromechanical brake system based on enhanced reaching law," *IEEE Access*, vol. 9, pp. 19506–19515, 2021, doi: 10.1109/ACCESS.2021.3052944.
[20] X. Song and Z. Sun, "Pressure-based clutch control for automotive transmissions using a sliding-mode controller," *IEEE/ASME Trans. Mechatronics*, vol. 17, no. 3, pp. 534–546, Jun. 2012.
[21] S. Kwon, S. Lee, J. Lee, and D. Kum, "Accurate state estimation for electro-mechanical brake systems," *J. Electr. Eng. Technol.*, vol. 14, no. 2, pp. 889–896, Mar. 2019, doi: 10.1007/s42835-019-00124-x.
[22] C. F. Lee and C. Manzie, "Near-time-optimal tracking controller design for an automotive electromechanical brake," *Proc. Inst. Mech. Eng., I, J. Syst. Control Eng.*, vol. 226, no. 4, pp. 537–549, Apr. 2012.
[23] C. F. Lee and C. M. C. Line, "Explicit nonlinear MPC of an automotive electromechanical brake," *IFAC Proc. Volumes*, vol. 41, no. 2, pp. 10758–10763, 2008.
[24] Y. Li, T. Shim, D.-H. Shin, S. Lee, and S. Jin, "Control system design for electromechanical brake system using novel clamping force model and estimator," *IEEE Trans. Veh. Technol.*, vol. 70, no. 9, pp. 8653–8668, Sep. 2021.

[25] Z. Xu and C. Gerada, "Enhanced force estimation for electromechanical brake actuators in transportation vehicles," *IEEE Trans. Power Electron.*, vol. 36, no. 12, pp. 14329–14339, Dec. 2021.
[26] S. Eum, J. Choi, S.-S. Park, C. Yoo, and K. Nam, "Robust clamping force control of an electro-mechanical brake system for application to commercial city buses," *Energies*, vol. 10, no. 2, p. 220, Feb. 2017, doi: 10.3390/en10020220.
[27] S. Formentin, G. Rallo, and S. M. Savaresi, "Data-driven clamping force control for an electric parking brake without speed measurement," in *Proc. IEEE Conf. Decis. Control (CDC)*, Miami Beach, FL, USA, Dec. 2018, pp. 5128–5133.
[28] Z. Xu and C. Gerada, "Enhanced estimation of clamping-force for automotive EMB actuators using a switching extended state observer," *IEEE Trans. Ind. Electron.*, vol. 71, no. 3, pp. 2220–2230, Mar. 2024, doi: 10.1109/TIE.2023.3265060.
[29] P. C. Krause, O. Wasynczuk, and S. D. Sudhoff, *Analysis of Electric Machinery and Drive Systems*, 2nd ed. Hoboken, NJ, USA: Wiley-IEEE, 2002.
[30] A. Dianov, "Comparison of feedback field-weakening techniques for synchronous machines with permanent magnets," *Vehicles*, vol. 5, no. 4, pp. 1671–1691, Nov. 2023, doi: 10.3390/vehicles5040091.
[31] S. Morimoto, K. Hatanaka, Y. Tong, Y. Takeda, and T. Hirasa, "Servo drive system and control characteristics of salient pole permanent magnet synchronous motor," *IEEE Trans. Ind. Appl.*, vol. 29, no. 2, pp. 338–343, Apr. 1993, doi: 10.1109/28.216541.
[32] S.-H. Kim, *Electric Motor Control : DC, AC and BLDC Motors*, 1st ed. Amsterdam, The Netherlands: Elsevier Science, 2017.

SEUNGKOO BAEK was born in 1975. He received the B.S. and M.S. degrees from Chungbuk National University, in 2001 and 2003, respectively, and the Ph.D. degree from Ajou University, in 2017.

From 2003 to 2005, he was a Hardware Development Engineer with SIEMENS Automotive. Since 2005, he has been a Senior Researcher with the Advanced Railroad Vehicle Division, Korea Railroad Research Institute (KRRI). His research interests include high-speed train, traction motor design and control, electromechanical brake systems, and power converter.